

Spatial decoherence of pulsed broad-area vertical-cavity surface-emitting lasers

Michael Peeters, Guy Verschaffelt and Hugo Thienpont

*Department of Applied Physics and Photonics, Vrije Universiteit Brussel,
Pleinlaan 2, B-1050 Brussels, Belgium.*

michael.peeters@ieee.org

Shyam K. Mandre and Ingo Fischer*

*Institute of Applied Physics, Darmstadt University of Technology,
Schloßgartenstr. 7, D-64289 Darmstadt, Germany*

** Now with the Vrije Universiteit Brussel, Belgium.*

Martin Grabherr

U-L-M Photonics GmbH,

Albert-Einstein-Allee 45, D-89081 Ulm, Germany

Abstract: We report a strong reduction of spatial coherence of the emission of large aperture vertical-cavity surface-emitting lasers when they are driven by microsecond electrical pulses. We give evidence that this is due to a breakdown of the modal emission of these lasers. The spatial decoherence manifests itself in the formation of a Gaussian far field intensity distribution. The coherence radius we extract is 1.4 micrometer under these operating conditions, irrespective of the Fresnel number of the vertical-cavity surface-emitting laser. Finally, the spatial coherence properties can be varied by changing the pulse duration or pulse amplitude.

© 2005 Optical Society of America

OCIS codes: (140.5960) Semiconductor lasers (250.7260) Vertical cavity surface emitting lasers (030.1640) Coherence (030.40700) Modes

References and links

1. L. Mandel and E. Wolf, *Optical Coherence and Quantum Optics* (Cambridge Press, 1995).
2. T. E. Sale, *Vertical Cavity Surface Emitting Lasers*, Optoelectronic series; 2 (John Wiley&Sons inc., New York, 1995). ISBN 0 86380 174 9.
3. A. Valle and L. Pesquera, "Analytical calculation of transverse mode characteristics in vertical-cavity surface-emitting lasers," *J. Opt. Soc. Am. B* **19**, 1549–1557 (2002).
4. C. J. Chang-Hasnain, J. P. Harbison, G. Hasnain, A. C. Vonlehmen, L. T. Florez, and N. G. Stoffel, "Dynamic, polarization, and transverse-mode characteristics of vertical cavity surface emitting lasers," *IEEE J. Quantum Electron.* **27**, 1402–1409 (1991).
5. P. Debernardi, G. P. Bava, C. Degen, I. Fischer, and W. Elsässer, "Influence of anisotropies on transverse modes in oxide-confined VCSELs," *IEEE J. Quantum Electron.* **38**, 73–84 (2002).
6. S. F. Pereira, M. B. Willemsen, M. P. van Exter, and J. P. Woerdman, "Pinning of daisy modes in optically pumped vertical-cavity surface-emitting lasers," *Appl. Phys. Lett.* **73**, 2239–2241 (1998).
7. S. Hegarty, G. Huyet, J. McInerney, and K. Choquette, "Pattern Formation in the Transverse Section of a Laser with a Large Fresnel Number," *Phys. Rev. Lett.* **82**, 1434–1437 (1999).
8. S. Hegarty, G. Huyet, P. Porta, J. McInerney, K. Choquette, K. M. Geib, and H. Hou, "Transverse-mode structure and pattern formation in oxide-confined vertical-cavity semiconductor lasers," *J. Opt. Soc. Am. B* **16**, 2060–2071 (1999).

9. K. Huang, Y. Chen, and L. Lai, "Observation of the Wave Function of a Quantum Billiard from the Transverse Patterns of Vertical Cavity Surface Emitting Lasers," *Phys. Rev. Lett.* **89**, 224,102 (2002).
10. T. Gensty, K. Becker, I. Fischer, W. Elsäßer, C. Degen, P. Debernardi, and G. P. Bava, "Wave Chaos in Real-World Vertical-Cavity Surface-Emitting Laser," *Phys. Rev. Lett.* **94**, 233,901 (2005).
11. S. Barland, F. Marino, M. Giudici, J. Tredicce, and S. Balle, "In situ measurement of cavity length variations across the transverse section of broad-area vertical-cavity surface-emitting lasers," *Appl. Phys. Lett.* **83**, 2303–2305 (2003).
12. M. C. Cross and P. C. Hohenberg, "Pattern formation outside of equilibrium," *Rev. Mod. Phys.* **65**, 851–1124 (1993).
13. A. Schell, "A Technique for the Determination of the Radiation Pattern of a Partially Coherent Aperture," *IEEE Trans. Antennas Propag.* **AP-15**, 187–188 (1967).
14. E. Collett and E. Wolf, "Is complete spatial coherence necessary for the generation of highly directional light beams?" *Opt. Lett.* **27**, 27–29 (1978).
15. M. von Waldkirch, P. Lukowicz, and T. Gerhard, "Effect of light coherence on depth of focus in head-mounted retinal projection displays," *Optical Engineering* **43**, 1552–1560 (2004).
16. M. Grabherr, R. Jäger, R. Michalzik, B. Weigl, G. Reiner, and K. J. Ebeling, "Efficient Single-Mode Oxide-Confining GaAs VCSEL's Emitting in the 850-nm Wavelength Regime," *IEEE Phot. Tech. Lett.* **9**, 1304–1306 (1997).
17. M. Grabherr, M. Miller, R. Jäger, R. Michalzik, U. Martin, H. J. Unold, and K. J. Ebeling, "High-Power VCSEL's: Single Devices and Densely Packed 2-D-Arrays," *IEEE J. Sel. Top. Quantum Electron.* **5**, 495–502 (1999).
18. M. Miller, M. Grabherr, R. King, R. Jäger, R. Michalzik, and K. J. Ebeling, "Improved Output Performance of High-Power VCSELs," *IEEE J. Sel. Top. Quantum Electron.* **7**, 210–216 (2001).
19. W. Nakwaski, "Thermal aspects of efficient operation of vertical-cavity surface-emitting lasers," *Opt. Quantum Electron.* **28**, 335–352 (1996).
20. C. Degen, I. Fischer, and W. Elsäßer, "Thermally induced local gain suppression in vertical-cavity surface-emitting lasers," *Appl. Phys. Lett.* **76**, 3352–3354 (2000).
21. F. Zernike, "The concept of degree of coherence and its applications to optical problems," *Physica* **5**, 785–795 (1938).
22. M. Born and E. Wolf, *Principles of optics, 7th Edition* (Cambridge Press, 1999).
23. A. W. Snyder and J. D. Love, *Optical Waveguide Theory* (Chapman & Hall, London, 1983).
24. Q. Lin and L. Wang, "Generation of partially coherent laser beam directly from spatial-temporal phase modulated optical resonators," *J. Modern Opt.* **50**, 743–754 (2003).
25. S. V. Kukhlevsky and L. Kozma, "Optical characteristics of pulsed capillary gas lasers with waveguide resonators," *Opt. Commun.* **115**, 425–428 (1995).
26. R. Tommasini, S. Insam, and E. Fill, "Coherence properties of an amplified spontaneous emission laser: experiments on a 10 Hz vacuum-ultraviolet H_2 -laser," *Opt. Commun.* **180**, 277–283 (2000).

1. Introduction

The coherence properties of light [1] and in particular of lasers are of great fundamental importance but also play an essential role in applications. For lasers with a high Fresnel number, the loss of full spatial coherence is usually due to the coemission of multiple mutually incoherent transverse modes, which are individually fully spatially coherent. One particular type of semiconductor lasers with a high Fresnel number are broad-area vertical-cavity surface-emitting lasers (VCSEL). VCSELs receive a lot of interest nowadays because of their interesting physical properties as well as their advantages for applications [2]. Due to the extremely short cavity length of the order of one wavelength, these lasers inherently emit in a single longitudinal mode. For a small enough aperture diameter of a few μm , the VCSEL cavity will only support the fundamental transverse mode. To increase the available output power, broad-area devices are used which easily become multimode with in general a very complex transverse mode structure. The description of the emission in continuous wave operation (CW) of such multimode VCSELs is often described by a model with a superposition of modes [3–6]. Nonetheless, some studies have shown that a VCSEL under CW operation can show complex pattern formation [7, 8] and even be described as a quantum billiard [9, 10] when the homogeneity of the device is sufficiently high [11] and the system has sufficient spatial extent.

In this paper, we show that when a broad-area VCSEL is driven by a strong current pulse, the modal description of the emission breaks down. Instead our experimental results demon-

strate a VCSEL behaving in the large system limit [12] as a quasi-homogeneous Schell-model source [13, 14] exhibiting a perfect Gaussian far field emission. By tuning the pulse duration and amplitude, we can significantly change the spatial coherence of these VCSELs. Our results show a simple way to generate partially coherent, highly directional beams. Sources with a reduced degree of spatial coherence may find many applications [1], e.g. they have been proposed as a way to increase the image quality and the depth of focus [15] in imaging systems. The realization of Gaussian far fields with large aperture devices has perspectives for several applications where the beam profile is essential, e.g. for printing. Moreover, a significant speckle reduction can be expected, making these devices attractive for projections systems. Other applications include illumination for night vision systems and range finders.

2. Observations

The devices used in our investigations are large aperture native oxide [16] confined VCSELs with a Fresnel number of the order of several hundreds to thousands, emitting at wavelengths around $\lambda = 840\text{nm}$ as described in detail in [17, 18]. For CW operation, the devices are driven by a low noise current source; in pulsed operation, we use a pulse generator with a rise time of 20ns. In all cases, the VCSELs are mounted on a temperature controlled heat sink (set at 30 degrees Celsius for all the experiments). The time averaged near field images of the emission were collected by a 12-bit digital camera, using a 40x microscope objective with a numerical aperture of 0.6 for the imaging. For imaging the time averaged far fields we have used a diffusive screen [8]. Unless stated otherwise, measurements shown here were performed on VCSELs with a $50\mu\text{m}$ diameter aperture, with a Fresnel number of order 10^3 . The results are reproducible for all nine $50\mu\text{m}$ diameter devices investigated.

For these $50\mu\text{m}$ aperture devices, exhibiting threshold currents of 15 mA, the maximal CW output power is 40mW when driven at a current of 80mA. The main limiting factor is thermal roll-over [19] because of the decreasing recombination efficiency caused by increasing re-emission of carriers [20], and increasing detuning between the cavity resonance and the gain maximum, both due to Joule heating in the cavity. The peak output power can be increased by pulsing the current sent through the device with a low duty cycle, as in that case the heat has time to dissipate. We observe pulse powers of up to 200mW (limited by our pulse generator) at a duty cycle of up to 10%. Such power levels and the associated pulse lengths are typical of what is required for the aforementioned printing application.

In Fig. 1, we show the time average over the pulses of the near (a,c,e) and far (b,d,f) fields of the $50\mu\text{m}$ aperture VCSELs. One can see that under CW operation at a drive current of 39 mA (Fig. 1(a)), the near field consists of a multitude of high order Laguerre-Gauss modes, dominated by a ring structure of daisy modes $LG_{l,0}$ ($l \gg 40$). The far field (or Fraunhofer diffraction zone) shown in Fig. 1(b) mirrors this modal structure and can be matched to the Fourier transform of the near field modal composition. The low intensity at the center is due to a phase singularity of the LG modes for $l > 0$ (only the lowest order Laguerre-Gauss is nonzero in the center). In the center of the near field, some patterns with a length scale of a few μm can be seen. They may be the superposition of Fourier modes as reported in [7, 8].

For a pulse of $1\mu\text{s}$ duration and 39mA amplitude, the near and far fields are shown in Fig. 1(c) and 1(d). The near field is still dominated by a ring structure as in the CW case, albeit slightly more blurred, but the far field has developed a local maximum in the center. Some remnants of the CW modal structure can still be seen at large angles, but spectral analysis shows that the maximum in the center is not due to the sudden appearance of the lowest order Laguerre-Gauss mode $LG_{0,0}$.

When increasing the pulse amplitude to 320mA, with the VCSEL emitting 200mW of peak power, the near field (Fig. 1(e)) only suffers more blurring of the ring. However the far field

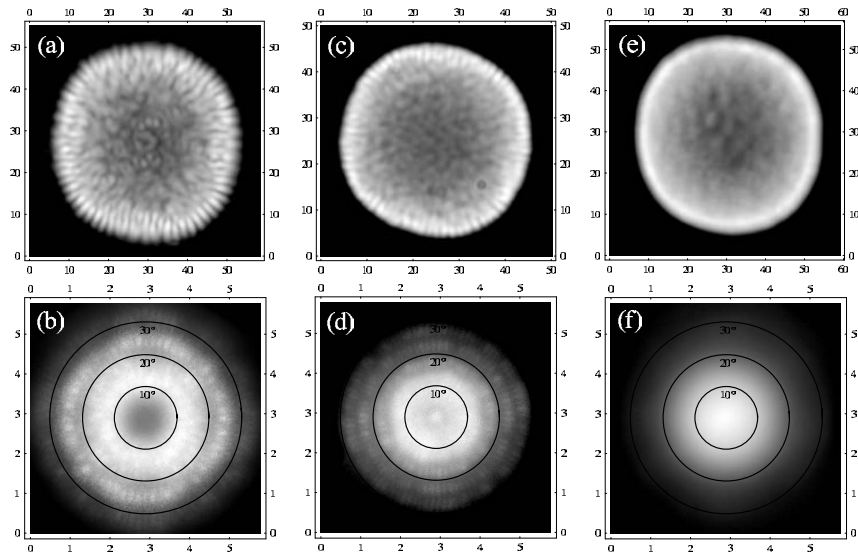


Fig. 1. An overview of the normalized intensity distribution in the near and far field. The intensity scale is logarithmic. Panels (a) and (b) depict the near and far fields in the CW case at an injection current of 39mA. Panels (c) and (d) show the near and far fields in the pulsed case at a pulse amplitude of 39mA, a pulse length of 1 μ s and a duty cycle of 2 percent. Panels (e) and (f) depict the near and far fields in the pulsed case at a pulse amplitude of 320mA, other parameters remain the same. The scale is in μ m for the near fields, in cm for the far fields. Angles correspond to the full opening of the cones.

(Fig. 1(f)) has drastically changed into a Gaussian profile. Figure 2 depicts a cut through this far field emission profile together with an almost perfect Gaussian fit corresponding to a full opening angle of 22 degrees. This divergence of the beam neither matches with what would be expected from fundamental mode emission of such an aperture, nor from a Laguerre-Gauss superposition. The far field, measured in Fig. 2 would be normally associated with a single mode laser with a beam waist radius of 1.4 μ m.

To get insight into the dynamics of this phenomenon, we have sampled both the near and far field with a multimode fiber coupled to a 2.4 GHz bandwidth photodiode and a 4 GHz bandwidth sampling oscilloscope (Tektronix CSA 7404). Under the same conditions as in the above experiments, no fast intensity dynamics other than the envelope of the current pulse were observed. In addition, snapshots of both the near and far field at different times within the pulse were taken with a 200 ps minimum exposure time intensified CCD camera (4 Picos), showing no discernible differences during the emission of the Gaussian far field. Thus we can exclude dynamical effects slower than 200 ps as a relevant mechanism. Finally, a linear polarizer was inserted into the beam and we have found no polarization dependence of the observed Gaussian intensity profiles.

3. Interpretation

A clue as to the origin of this Gaussian far field emission can be found in the seminal papers of Zernike [21], Schell [13] and Collett and Wolf [14]. They showed that for nearly monochromatic sources ($\Delta\lambda \ll \lambda$) of arbitrary stationary spatial coherence, the far field pattern is determined by the Fourier transform of the product of the autocovariance $C(\vec{\rho})$ of the aperture

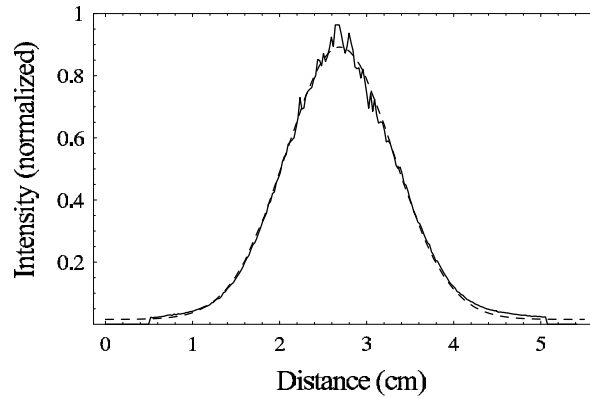


Fig. 2. A transverse cut through the far field of the pulsed device, corresponding to case (f) of Fig. 1. The solid line is the measurement, the dashed line a Gaussian fit with a estimated variance of 3.2×10^{-4} . The full far field opening is 22 degrees ($1/e^2$).

amplitude function with the complex degree of source coherence $\mu^{(0)}(\vec{\rho}_1, \vec{\rho}_2) \equiv g^{(0)}(\vec{\rho}_2 - \vec{\rho}_1)$. Indeed, the radiant intensity $J(\vec{s})$, i.e., the intensity distribution in the far field direction \vec{s} (neglecting frequency and polarization dependencies) is in the paraxial domain proportional to

$$J(\vec{s}) \sim \int_A g^{(0)}(\vec{\rho}) C(\vec{\rho}) e^{i\vec{f} \cdot \vec{\rho}} dA \quad (1)$$

where the integration is performed over the near field coordinate $\vec{\rho}$ and the spatial frequency \vec{f} is related to the projection \vec{s}_\perp of the direction \vec{s} on the observation plane, $\vec{f} = (2\pi/\lambda)\vec{s}_\perp$ [1, 13, 14, 21].

Quasi-homogeneous sources are partially coherent sources whose effective coherence area is much smaller than the aperture area. Under such conditions, Eq. (1) shows that the far field is primarily determined by the Fourier transform of the coherence function $g^{(0)}(\vec{\rho})$ of the near field, not by the near field amplitude distribution [1]. This fact simplifies greatly the determination of the coherence area of the source: if the far field intensity distribution J is observed to be Gaussian, the complex degree of source coherence $g^{(0)}$ must also be Gaussian and depends only on the coordinate difference ρ :

$$g^{(0)}(\rho) = \exp(-\rho^2/2\xi^2). \quad (2)$$

The intensity distribution in the far field is then given by [1]

$$\begin{aligned} J(\theta) &= J(0) \exp\left(-\frac{1}{2}\left(\frac{2\pi}{\lambda}\xi \sin\theta\right)^2\right) \\ &\simeq J(0) \exp(-2\theta^2/\theta_{1/e^2}^2) \end{aligned} \quad (3)$$

where θ is the angle of \vec{s} with respect to the beam center, and the approximate form is valid for paraxial angles. A fully coherent single fundamental transverse mode laser would have the same far field intensity distribution. Nevertheless it does not originate from such a source [14]. By comparing Eqs. 2 and 3 it is clear that the rms width ξ of the degree of coherence at the source plane and the $1/e^2$ divergence angle θ_{1/e^2} are related by

$$\theta_{1/e^2} = \frac{\lambda}{\pi\xi}. \quad (4)$$

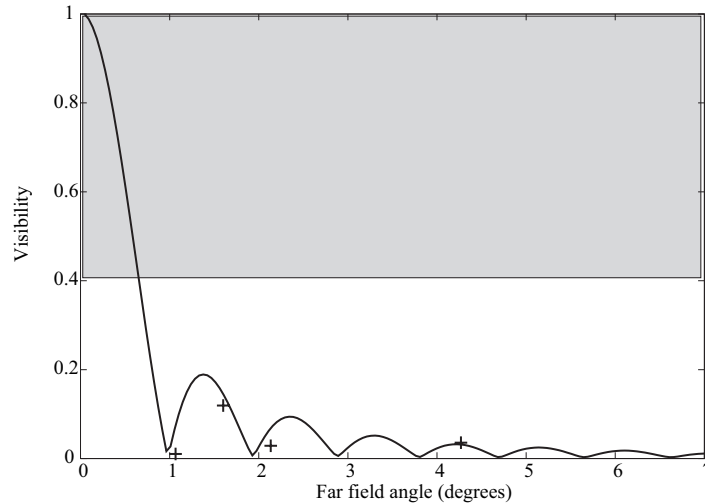


Fig. 3. The calculated angular coherence for a quasi-homogeneous source with the intensity distribution as in Fig. 1(e) is indicated by the solid line. The crosses are measurements at different slit separations. Measurements at slit separations larger than 7 degrees (outside of the plot range) show almost zero visibility. The shaded area corresponds to the measured visibility range for CW multimode emission.

Using Eq. (4) and the measured Gaussian far field we obtain a coherence radius ξ of $1.4\mu\text{m}$. The origin of this length scale is as yet not fully clear. Measurements on otherwise similar devices with aperture diameters ranging from 50 down to $14\mu\text{m}$ show that the divergence angle is *not* a function of the VCSEL's aperture size. This is consistent with the quasi-homogeneous property that the aperture does not influence the far field intensity distribution.

Additionally, quasi-homogeneous sources satisfy another interesting reciprocity relation: the far field angular degree of coherence $\mu^{(\infty)}(\vec{s})$ is given by the Fourier transform of the near field intensity distribution [1]. As a consequence and in order to check whether quasi-homogeneity is indeed the cause of the observed far field, we have measured the visibility of the fringes in a Young's interference experiment. To this end, the VCSEL was re-imaged with a magnification of 40 onto the surface of a CCD using an asphere with a focal length of 7 mm. The slits were placed directly behind the lens in the far field of the source at a distance of 32 cm from the CCD (corresponding to the far field of the image). This geometry has been chosen such that the fringe pattern matches the size of the CCD chip. The visibility is now a measure of the absolute value of the angular coherence $|\mu^{(\infty)}(\vec{s})|$ in the far field. Assuming the source to be quasi-homogeneous, we can calculate the angular coherence and visibility as a function of slit separation [1, 22] from the measured intensity distribution of the VCSEL. The first zero of the visibility then corresponds to a slit separation of $152\mu\text{m}$ (about 1 degree of separation). The calculated visibility together with measured values are shown in Fig. 3. The measured visibility matches well with the calculated values starting from the near field intensity, supporting again our assumption of quasi-homogeneity for driving conditions corresponding to Fig. 1(f).

In contrast, for modal emission obtained in CW operation (Fig. 1(b)) the measured visibilities always yielded values above 0.4 as indicated by the gray shaded area in Fig. 3. We do not provide a clear dependence, as in the case of modal emission the stationarity of $\mu^{(\infty)}(\vec{s}_1, \vec{s}_2)$ and hence the visibility with respect to the chosen directions is not a given. Hence, an angular or spatial coherence scale is not well defined at all pulse durations and amplitudes.

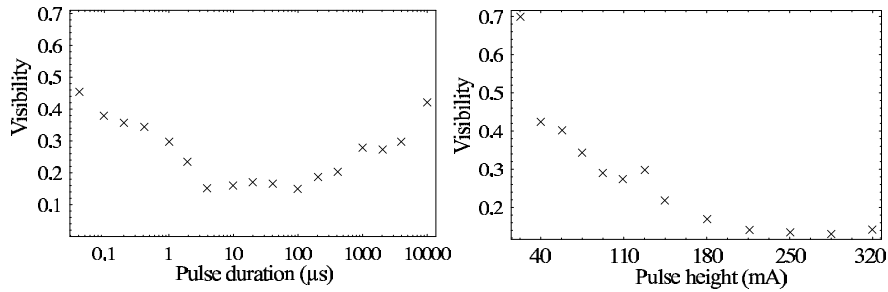


Fig. 4. A plot of the visibility of the fringes for different values of (a) the pulse duration at a pulse amplitude of 110mA, duty cycle 2%. (b) the pulse amplitude at a pulse duration of 1μs, duty cycle 2%

4. Transition

After verifying the quasi-homogeneity of the emitted beam in the case corresponding to Fig. 1(f), we have now chosen a slit separation of 150μm in order to clearly show the transition from the fully coherent to the quasi-homogeneous case. For fully coherent emission, we expect $V = 1$ (it is then independent of the angular separation) while for quasi-homogeneous emission, we expect $V = 0$. Other partially spatially coherent states, e.g. CW multimode emission, correspond to intermediate values. The results in dependence of pulse duration and amplitude are depicted in Fig. 4.

Starting with a fixed pulse amplitude of 110mA (Fig. 4(a)) and for small pulse durations, the visibility is maximal, indicating a high degree of angular coherence compared to the slit separation. Increasing the pulse duration, the visibility monotonically drops until a pulse duration of a few μs. For longer pulses, the visibility increases again to the starting value. For such long pulses, the far field is seen to consist of a mix of a Gaussian center with high order daisy modes superimposed (not shown). The increase in visibility for long pulse durations is due to the reappearance of modal structures at long times. It turns out that we can relate the longest time scale before modes reappear to the thermal timescale. To this end, the wavelength shift $\Delta\lambda$ was measured as a function of the pulse duration T . It could be well fitted by a power law $\Delta\lambda(T) = Q(T/\tau)^b$ with a timescale τ of 1.56μs, an exponent b of 0.13 and a prefactor Q of 2.38nm, similar to what has been reported before [17]. In Fig. 4(a) the visibility indeed levels off at this timescale. Also, when we look at the spatially resolved total chirp $\Delta\lambda(\rho, T) = \lambda(\rho, T) - \lambda(\rho, 0)$ in the pulsed case, we find variations of up to 0.5nm across the cavity for a pulse duration of 1μs and a pulse amplitude of 110 mA, indicating the presence of a pronounced thermal gradient.

Increasing the pulse amplitude results in a monotonous decrease of the visibility at fixed pulse duration (Fig. 4(b)). Shallow or short pulses exhibit almost fully coherent emission, while for high amplitude pulses visibility gets lost quickly. We have systematically studied the visibility under variation of pulse amplitude and duration, the results of which are shown in Fig. 5. It exhibits a large region of low angular coherence. This is exactly the region in which we also observe the Gaussian far field. We thus demonstrate that we can change the emission from multimodal to quasi-homogeneous by varying the pulse parameters.

5. Origin

Having demonstrated that the spatial coherence properties are related to thermally induced changes of optical cavity properties, we will at the present substantiate that in VCSELs there is

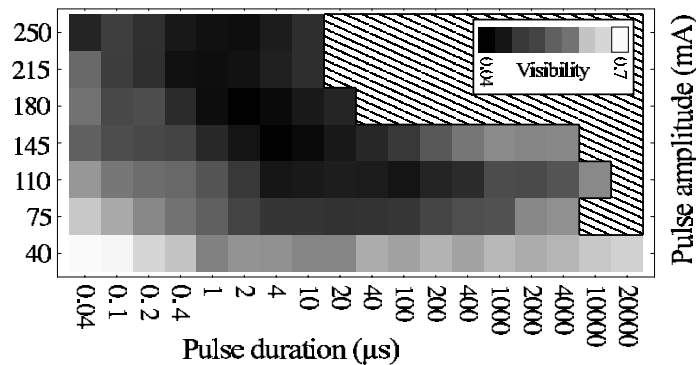


Fig. 5. A density plot of the visibility of the fringes for different values of the pulse duration and pulse amplitude. The duty cycle was 2% in all cases. White means high visibility $C=0.7$ and black low $C=0.04$; the dashed area corresponds to points where we do not observe sustained laser operation for the entire pulse duration.

a generic physical mechanism causing this relationship.

We interpret the results as an inability of the VCSEL to relax to modal solutions satisfying the global boundary conditions in the presence of chirp and strong internal waveguiding. Instead it exhibits stimulated emission in *locally* coherent islands with a typical length scale of a few μm . Much as increasing the index difference between core and cladding in a waveguide increases the transient length [23], the presence of a phase profile due to the thermal lens increases the number of round trips needed to achieve full coherence [24, 25]. In addition, the cavity is expanding and therefore non-stationary during pulsed operation, causing strong thermal chirp. Even so, local islands are emitting in the stimulated emission regime during the chirping. The intensity profile for emission in these coherent islands is determined by the pump current profile, which is known to be strongly annular for large oxide confined devices due to the contact ring and current crowding [17]. Modal emission only reappears after a large multiple of the thermal time-scale when the chirp decreases again. Under CW operation, the system develops a static thermal profile and the laser can settle down and emit in *globally* determined modes.

We stress that it is the thermal lens causing an increase in the modal buildup time, allowing chirp to keep the cavity in a transient state which in turn causes the loss of spatial coherence. Since the material system and device structure described here are typical for VCSELs, this behavior is expected to be common for various VCSEL structures. Nonetheless we note that such quasi-homogeneous emission is uncommon in lasers without additional active or passive intra- or extra cavity elements [1, 24, 26]. A related phenomenon has been described in capillary waveguide lasers [25], where in contrast to our lasers a small number of round trips is at the origin of the low spatial coherence.

6. Conclusion

We have observed a strong reduction of the spatial coherence of oxide-confined multimode vertical-cavity surface-emitting lasers when pulsing the electric current sent through these devices. This partial decoherence leads to the formation of an unexpected Gaussian far field intensity distribution when pulsing in the μs regime. We show that the VCSEL can be described as a quasi-homogeneous Schell-model source (also called Collett-Wolf source) with a coherence radius of $1.4\mu\text{m}$, which in fact determines the far field intensity pattern. The decoherence is due to a collapse of the modal emission under certain driving conditions. Additionally, the spatial

coherence properties can be varied over a wide range by changing the pulse duration or pulse amplitude. Possible applications include the direct generation of partially coherent beams and increasing the directionality of multimode VCSEL beams.

Acknowledgments

MP and GV would like to thank IWT (project 030501) and Strobbe Graphics for financial support of applied research, Jari Turunen for proofreading the manuscript and Erik Stijns for his help in the set-up of the coherence measurements. GV gratefully acknowledges the financial support of FWO. Additional support was provided via the Interuniversity Attraction Pole programme IAP V-18 PHOTON.